



Article

Multi-Layer Material Characterization at Ka-Band Using Bayesian Inversion Method

Saleem Shahid ^{1,*}, Gian Guido Gentili ², Giancarlo Bernasconi ², Hamza Nawaz ³ and Ahsan S. Rana ¹¹ Department of Electrical and Computer Engineering, Air University, Islamabad 44000, Pakistan² Department of Electronics, Information, and Bio-Engineering, Politecnico di Milano, 20133 Milan, Italy³ School of Electrical, Information and Electronics Engineering, Shanghai Jiao Tong University, Shanghai 200240, China

* Correspondence: saleem.shahid@mail.au.edu.pk

Abstract: This paper presents the implementation of the Bayesian inversion method for the characterization and estimation of different dielectric material properties. The scattering parameters of single and multi-layer materials are measured using a free-space experimental setup using a standard gain horn antenna and a Vector Network Analyzer (VNA) at Ka-band (26–40 GHz). The relative permittivity, material thickness, and material positioning error are defined as model parameters and estimated using the observed (measured) data. The FR4 Epoxy, Rogers RT/Duriod 5880, and Rogers AD600 with different relative permittivities and thicknesses are used in the measurement setup. The results displayed good agreement between model parameters and estimated properties of the presented materials, while the corresponding eigenvectors provided a level of confidence in model parameter values. The results were compared with different reported techniques to showcase the possible use of the presented method in microwave imaging, non-destructive testing, and similar applications.

Keywords: material characterization; Bayesian inversion method; relative permittivity; material thickness; s-parameters; eigenvectors



Citation: Shahid, S.; Gentili, G.G.; Bernasconi, G.; Nawaz, H.; Rana, A.S. Multi-Layer Material Characterization at Ka-Band Using Bayesian Inversion Method. *Electronics* **2023**, *12*, 563. <https://doi.org/10.3390/electronics12030563>

Academic Editor: Christos J. Bouras

Received: 30 November 2022

Revised: 23 December 2022

Accepted: 3 January 2023

Published: 21 January 2023



Copyright: © 2023 by the authors. Licensee MDPI, Basel, Switzerland. This article is an open access article distributed under the terms and conditions of the Creative Commons Attribution (CC BY) license (<https://creativecommons.org/licenses/by/4.0/>).

1. Introduction

Dielectric measurement systems for material characterization at microwave and millimeter frequencies have been playing a vital role in various medical, security, and non-destructive testing applications for the last few decades [1–3]. Different types of dielectric measurement setups have been improved by enhancing the antenna focusing performance, experimental setups, signal processing algorithms, etc., in order to achieve ultra-wideband (UWB) scattering fields spectrum from the object or dielectric materials [3]. Microwave and millimeter frequency signals are widely used to record the s-parameters for further post-processing and estimation of electrical properties of the materials, particularly dielectrics. The dielectric material characterization has been divided into various types of measurements, which mainly depend on the nature of the characterization, i.e., (a) measurement in the narrow or broadband spectrum, (b) material under test (MUT) is low loss or high loss material, (c) measurement of either electrical or magnetic properties, etc. [2–5]. The free-space dielectric measurement method has been used widely over the years to efficiently extract the transmission and/or reflection scattering parameters from the MUT, which is placed between the transmit and receive antennas [5]. The free-space measurement method depends on a non-destructive evaluation technique in order to avoid physical contact with a sample and avoid the extra machining care needed for MUT [4].

The conventional free-space measurement methods for rock properties characterization have been experimented with by Bernasconi et al. [6]. Later, a low-loss dielectric measurement setup was also demonstrated at millimeter wave frequency bands [7] which provided a comprehensive uncertainty analysis for material characterization. Similarly, a method for the dielectric permittivity estimation using Brewster's angle and the magnitude

of the transmission and reflection coefficients measured from a reference metal and the MUT [8]. In contrast to the conventional free-space measurement methods for microwave, millimeter, or sub-millimeter frequencies, the dielectric properties of the low-loss and thinner materials have been estimated majorly from the envelopes of measured transmission and reflection spectra instead of the whole scattering parameters, unlike visible light or X-rays [9,10]. In most studies, only normal incidence interactions with materials are noticed to build the maximal and/or minimal envelopes. Many other interesting discussions on analytical analysis and derivations for the envelope method and its utilization in the dielectric measurement systems have been found in [11–13].

The time-domain Bayesian inversion method is one of the most accurate and time-efficient inversion methods, especially for reducing the uncertainties in estimating various materials' electrical and magnetic parameters [14,15]. This method is used to characterize dielectric material properties from the measured scattering parameters quantitatively. The Bayesian inversion method is also used to extract detailed information about the model parameters in terms of probability density. Later, this probability density can be used to measure the uncertainty in the assumed model parameters to build confidence in the observed data parameters [16]. Here, the joint interpretation approach is used to estimate the dielectric constant (ϵ_r), dielectric thickness (T_{d2}), and positioning error in the placement of dielectric material (T_{d1}) from the observed data set [17]. This paper applies the Bayesian inversion method for the estimation of the mentioned properties of single and multi-layer dielectric materials. Initially, a calibration procedure is employed, in which the scattering data is measured by placing the reference ground plane at a finite distance from the transmitting horn antenna.

After measuring the scattering from the reference ground, the MUT is introduced, and the scattering parameters are measured. The material characterization is treated as the inverse problem, and the parameter uncertainties are accounted for in the inversion method [18–20]. An iterative inversion procedure minimizes the residual between the assumed data and measured (observed) data, as shown in Figure 1. The measurements are carried out with a standard gain horn antenna at Ka-band. The rest of the paper is organized as Section 2 describes the Bayesian inversion method. Section 3 presents the measurement results in terms of calculated model parameters and their corresponding confidence in estimation, while Section 4 concludes the paper.

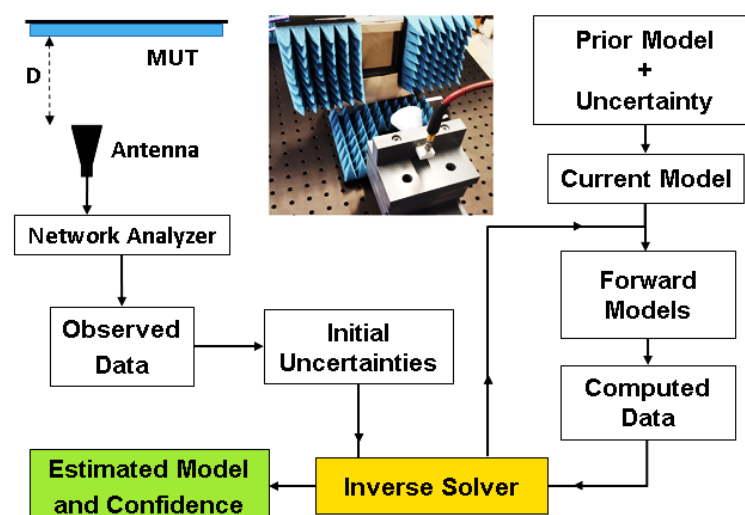


Figure 1. Bayesian inversion procedure after scattering parameters extraction.

2. Bayesian Inversion Method

The uncertainties in material properties like dielectric constant, MUT thickness, and positioning have been reduced significantly using Bayesian inversion. The free space measurements are carried out where the MUT with a grounded surface is placed at a fixed

distance from the transmitting antenna. Electrical and physical properties are parameters related to heterogeneous well-log observations: they are fundamental in the integration of measurements to enhance the characterization of materials [4,5]. The probabilistic approach is used to implement the solution [6], where we have found the probability densities, solid materials model and data uncertainties, and the prior model for the set of desired material properties. The detailed derivation of constitutive equations is available in [11]. MATLAB is used to implement the Bayesian inversion method.

The relative permittivity (ϵ_r) of the material, the thickness of each layer (T_{d2}), and the positioning error in the measurement setup (T_{d1}) are represented in the mathematical model. Constitutive equations relate the equivalent medium of observed data (D_{obs}) to the model parameters ϵ_r , T_{d1} , and T_{d2} , where $\epsilon_r = [\epsilon_{r1}, \epsilon_{r2}, \dots]^T$ and $T_{d2} = [T_{d21}, T_{d22}, \dots]^T$ are the vectors of single as well as multi-layer materials.

$$D_{obs} = g(\epsilon_r, T_{d1}, T_{d2}) \tag{1}$$

The model mentioned above can also represent cases in which the material spacing from the transmitting antenna is not exactly known. In that case, an additional “air” material is introduced, and its thickness is incorporated into the model. The cross-property relations are useful in estimating one property of material from another, e.g., T_{d2} can be estimated easily, which could be further used to estimate T_{d1} .

2.1. Current and forward Models

Using Tarantola’s notation [4], a vector Z_m is defined for the unknown model parameters of MUT, which are included in model space M1;

$$m = [\epsilon_r, T_{d1}, T_{d2}, \dots]^T \tag{2}$$

The set of initial model parameters is represented by a priori model M_{priori} and a covariance matrix C_M in order to record the uncertainties in M_{priori} . Another vector Z_o is defined for the observed data in the form of reflection coefficients (S_{11}) from scattering measurements, which is included in the model space M2,

$$d = [D_{obs}]^T \tag{3}$$

Similarly, the covariance matrix C_o contains uncertainties in observed data. The forward model is defined as the prediction algorithm for accurate estimation of observed parameters which corresponds to the given model m , denoted as;

$$d = g(m) \tag{4}$$

where g is a non-linear vectorial function used to predict values of a physical system in each set of model parameters $m \in M1$, and the values of observed parameters $d \in M2$, represented as a set of equations $d_i = g_i(m_1, m_2, \dots)$. The forward model then calculates the approximations in modeling uncertainties and records them in matrix C_g . All the measurements contain uncertainties, and therefore, the data set can’t be described as the observed value but as a state of information extracted from an observed parameter. If we represent the $d = [d_1, d_2, \dots, d_n]$ as the set of observed data, then the measured data can be defined in terms of probability density $\rho D(d)$ for the observed data space M2.

2.2. Solution of the Inverse Problem

The prior probability density of model space M1 and data space M2 is defined as $\rho(d,m)$ for collective space $M1 \times M2$. The theoretical probability density is also described as $\rho_t(d,m)$ for the correlation between m and d . The information of prior and theoretical

probability densities is combined to get the posterior state of information. The posterior probability density $\sigma(d,m)$ is defined as;

$$\sigma(d,m) = \frac{k[\rho(d,m) \cdot (\rho_t(d,m))]}{\mu(d,m)} \tag{5}$$

where $\mu(d,m)$ represents the homogeneous state of information and k is a normalization constant. Once the posterior information in the $M2 \times M1$ space has been defined, the posterior information in the model space is given by the marginal probability density as;

$$\sigma_M(d,m) = \int_{M2} d_d \sigma(d,m) \tag{6}$$

while the posterior information in the data space is given by

$$\sigma_D(d,m) = \int_{M1} d_m \sigma(d,m) \tag{7}$$

The solution to the inverse problem is hidden in the probabilistic framework, and it can be derived through the iterative procedure. The forward model is linearised around the current model (M_k) and gives a new model (M_{k+1}) by using the Jacobian matrix J_k , which is comprised of the derivatives of the forward model equation and current model parameters.

$$M_{k+1} = M_{\text{priori}} - [J_k^T C_d^{-1} J_k + C_M^{-1}]^{-1} J_k^T C_d^{-1} \cdot [(g(M_k) - d) - J_k(M_k - M_{\text{priori}})] \tag{8}$$

Here, matrix C_d stores the uncertainties of both observed and modeling data, with the Gaussian assumption of $C_d = C_o + C_g$ [9]. After the 1st iteration, the current estimated model M_1 is set to a priori model M_{priori} . The solution is obtained by upgrading the current model until the posterior probability density of the model is maximized [11]. The iterative algorithm stops when;

$$M_{i,k+1} - M_{i,k} < \epsilon, \forall i = 1, \dots, Z_m \tag{9}$$

The uncertainty of the solution is stored in matrix $C_{M,\text{post}}$, which computes the overall uncertainties of the solution as;

$$C_{M,\text{post}} = [J_k^T C_d^{-1} J_k + C_M^{-1}]^{-1} \tag{10}$$

2.3. Analysis of Uncertainties

The singular value decomposition analysis [9] is performed on the uncertainty of observed data by using the same constitutive equations around the reference M_{priori} model m_0 ;

$$m_0 = [\epsilon_{r_i}^0 \ T_{d2_i}^0]^T \tag{11}$$

$$d - d_0 = g(m - m_0) \tag{12}$$

Here, d_0 is the data vector generated by the reference M_{priori} model using the constitutive equations, whereas J is the Jacobian matrix which contains all the first-order partial derivatives of the forward model [9] with respect to the model parameters.

$$J = \left[\frac{dD_{\text{obs}}}{d\epsilon_r} \quad \frac{dD_{\text{obs}}}{dT_{d1}} \quad \frac{dD_{\text{obs}}}{dT_{d2}} \right] \tag{13}$$

The singular value decomposition of g is [3,9];

$$J = A\Lambda B^T \tag{14}$$

Here, matrix A contains the eigenvectors of data space while the Λ is the diagonal matrix of all the singular values. The Λ matrix represents the magnitude of data due to the

normalized variation along the eigenvectors axis in the model space. The matrix B contains the eigenvectors of the model space, where linear pairs of the unknown model parameters ϵ_r , T_{d1} , and T_{d2} are formed by developing the model space's orthogonal basis [11].

3. Material Parameter Estimation and Analysis

3.1. Single-Layered Materials

In the case of single-layer MUT measurements, one-sided copper (PEC) coated materials are used. The scattering parameters of different single-layer materials are measured at different distances (S_D) from the transmitting antenna, such as 6, 8, 10, 13, and 18 cm. The first single-layer material presented with the given properties of FR4 Epoxy, $\epsilon_r = 4.4$ and $T_{d2} = 1.52$ mm. Figure 2a shows the ϵ_r vs. T_{d1}/T_{d2} graph where the ϵ_r value of corresponding thickness is plotted for each value of S_D . The relative permittivity of FR4 Epoxy is estimated between 4.465 and 4.588, and it is observed that increasing the value of S_D decreases the accuracy of the estimated ϵ_r value. The positioning error remained less than -0.1 mm, whereas the thickness of FR4 Epoxy is estimated between 1.518 and 1.429 mm for each value of S_D . The absolute values of eigenvectors in the model space are shown in Figure 2b, where the eigenvectors are stacked on the horizontal axis (left to right) with decreasing singular values, whereas the model parameters are stacked on the vertical axis (bottom to top). From the legend bar, the blue color shows the lowest confidence, and the yellow color shows the highest confidence on the model parameters. From Figure 2b, T_{d2} acquired the highest confidence (associated with the first eigenvector), then T_{d1} (second eigenvector), and finally ϵ_r (third eigenvector).

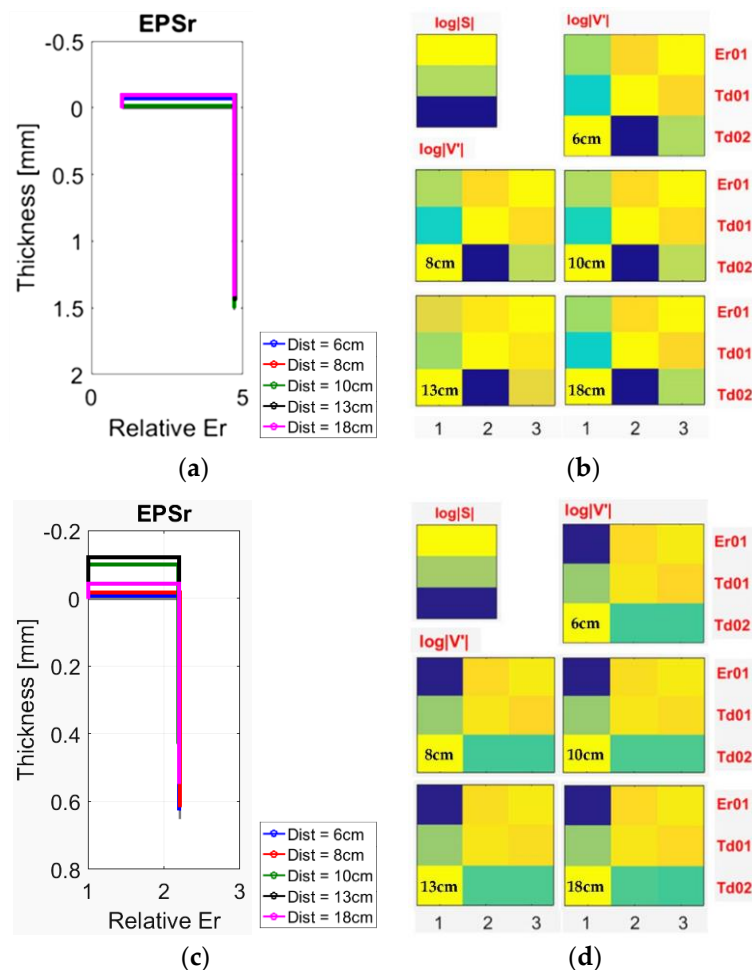


Figure 2. The parameters estimation for single-layer materials.

The second single-layered material presented is Rogers RT/Duriod 5880 with $\epsilon_r = 2.2$ and $T_{d2} = 0.65$ mm. Figure 2c shows the ϵ_r vs. T_{d1}/T_{d2} graph for each S_D value. The positioning error, T_{d1} , is much lower (-0.007 mm) for the case of 6 cm, whereas it is -0.034 mm for the case of 13 cm. The thickness of Roger RT/Duriod 5880 is estimated to be between 0.642 and 0.612 mm. From Figure 2d, T_{d2} shows the highest confidence (associated with the first eigenvector), then T_{d1} (second eigenvector), and finally ϵ_r (third eigenvector). In these free space measurements, the solution to the inversion problem found higher confidence in the thickness of the MUT compared to the ϵ_r . It can be observed that, for all the other single-layer materials, the ϵ_r decreases with increasing the distance S_D . Table 1 summarizes the estimation of the parameters for single-layer materials.

Table 1. Summary of Single-layer Material Estimation.

Materials Parameters		Distance b/w Tx and MUT				
		6 cm	8 cm	10 cm	13 cm	18 cm
FR4 Epoxy	ϵ_r	4.465	4.469	4.516	4.572	4.588
	T_{d1} (mm)	-0.073	-0.082	-0.012	-0.091	-0.096
	T_{d2} (mm)	1.514	1.518	1.511	1.432	1.429
Rogers RT/Duriod 5880	ϵ_r	2.192	2.201	2.187	2.188	2.189
	T_{d1} (mm)	-0.007	-0.011	-0.019	-0.031	-0.034
	T_{d2} (mm)	0.642	0.640	0.632	0.618	0.612

3.2. Multi-Layered Materials

The free space measurements are carried out at Ka-band for three different multi-layer cases, which are comprised of two dual-layer cases and one tri-layer case. All the multi-layer cases presented above are measured at a distance of 10 cm from the transmitting antenna. The dual-layer cases show a good estimation of model parameters with low positioning error, whereas the tri-layer case showed a relatively higher positioning error with a suitable estimation of model parameters.

The information about model parameters in terms of probability density [4,5] is used to find uncertainties in the model to build confidence in measured data. The echo response of both computed and observed data is compared, and ambiguities have been reduced between the MUT thicknesses and positioning error, where the initial value of positioning error is set to 0. Three materials used in the measurement campaign have given material properties of FR4 Epoxy, $\epsilon_r = 4.4$ and $T_{d2} = 1.52$ mm/0.78mm, Rogers RT/Duriod 5880 with $\epsilon_r = 2.2$ and $T_{d2} = 0.65$ mm, and Rogers AD600 with $\epsilon_r = 6.15$ and $T_{d2} = 0.5$ mm. In these cases, the desired probability density is achieved with maximum third model iterations (M_3) from the prior model (M_{priori}). The minimum residual percentage of 6.2% is found for case 2 at the second model iteration (M_2), but the estimation of model parameters is in good agreement with prior model parameters. The residual response for tri-layer materials was below 15% at the third model iteration (M_3). Figure 3 shows the ϵ_r vs. T_{d1}/T_{d2} graph where the ϵ_r value of each layer with respect to the corresponding thickness is plotted for all the multi-layer cases. The positioning error is -0.027 mm for the tri-layer case, but still, the inversion method was able to estimate model parameters correctly. For both dual-layer cases, the positioning error between -0.012 and -0.018 mm and the model parameters was estimated with less than 5% tolerance.

The Jacobian matrix J is calculated for all the multi-layer cases, and the confidence in model parameters has been found compared to the given model space. The absolute values of eigenvectors in the model space are shown in Figure 4, where eigenvectors are ordered (left to right) with decreasing singular values. It is observed that, for the first two-layer case (left side), T_{d21} was the parameter with the highest confidence (associated with the first eigenvector), then T_{d22} (second eigenvector), T_{d1} (third eigenvector), ϵ_{r2} (fourth eigenvector) and finally, ϵ_{r1} (fifth eigenvector), whereas, for the two-layer case (right side),

T_{d22} is the parameter with the highest confidence (associated to the first eigenvector), then T_{d21} (second eigenvector), ϵ_{r2} (third and fourth eigenvector), and finally, T_{d1} (fifth eigenvector). For the case of tri-layer material, T_{d22} was the parameter with the highest confidence (associated with the first eigenvector), then T_{d21} (second eigenvector), T_{d23} (third eigenvector), ϵ_{r3} (fourth eigenvector), ϵ_{r4} (fifth eigenvector) and finally, T_{d1} and ϵ_{r1} (sixth and seventh eigenvector respectively). The multi-layer cases, along with the estimated model parameters, are tabulated in Table 2.

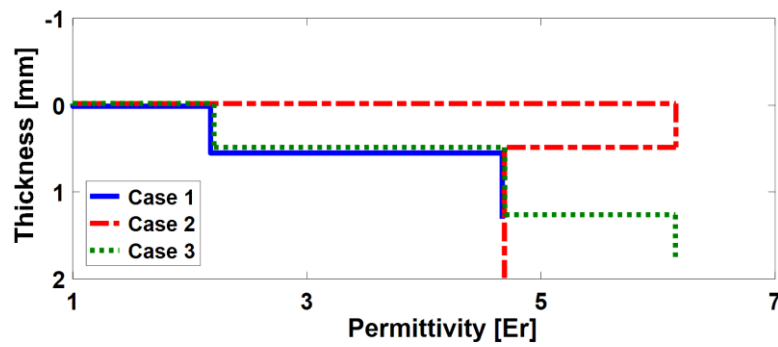


Figure 3. Estimated values of model parameters.

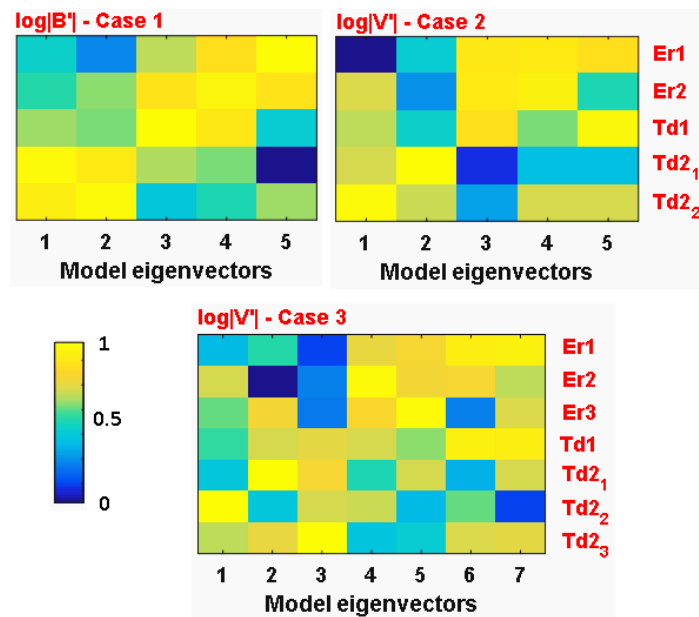


Figure 4. Confidence in the estimated model parameters.

Table 2. Summary of Multi-layer Material Estimation.

Cases	Materials	ϵ_r	T_{d2} (mm)	T_{d1} (mm)
Case 1	Rogers RT/Duriod 5880 FR4 Epoxy	ϵ_{r1}	2.177	T_{d21} 0.638
		ϵ_{r2}	4.468	T_{d22} 0.759
Case 2	Rogers AD600 FR4 Epoxy	ϵ_{r1}	6.152	T_{d21} 0.504
		ϵ_{r2}	4.487	T_{d22} 1.503
Case 3	Rogers RT/Duriod 5880	ϵ_{r1}	2.487	T_{d21} 0.631
	FR4 Epoxy	ϵ_{r2}	4.690	T_{d22} 0.776
	Rogers AD600	ϵ_{r3}	6.147	T_{d23} 0.501

Figure 5 shows the overview of the confidence level on the estimated parameters. In the free space measurements, the inversion problem has found higher confidence in

the thicknesses (T_{d2}) of the MUT as compared to dielectric constants (ϵ_r) of the different layers. In this regard, it is imperative to mention that many other multi-layer cases have been evaluated in order to validate the inversion method, but only the results of a few known materials are presented to promote the reproducibility of the experiments and the corresponding Bayesian inversion method.

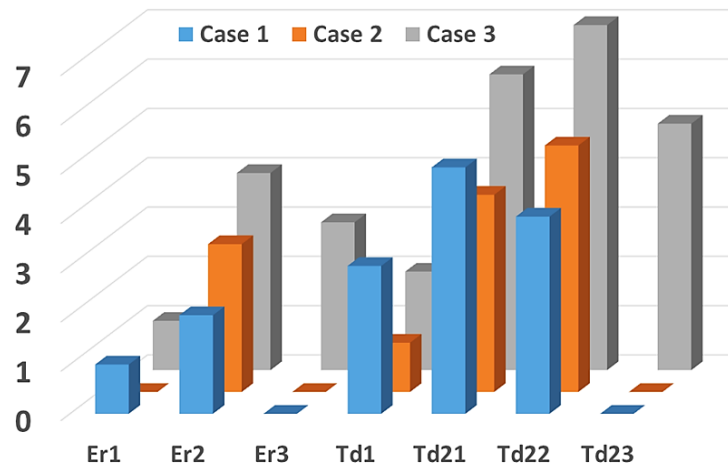


Figure 5. Comparison of confidence level in the estimated model parameters.

The presented results are also compared with some of the recently reported material properties estimation methods. The loaded waveguide technique and clamped waveguide technique have been used in [11], EM simulations were conducted to measure the scattering (S) parameters in [12], and the reflection measurements of a loaded and unloaded CPW (co-planar waveguide) line sample holder were conducted in [13]. The tabular comparison with these techniques is presented in Table 3. The presented Bayesian inversion method showed a lower percentage error in the estimation of relative permittivity as compared to others. Additionally, the presented inversion method estimates (a) the relative permittivity of multi-layer materials, (b) the thickness of the materials, and (c) the positioning error in the placement of the material under test.

Table 3. Comparison of the Presented Inversion Method with Other Techniques.

Reference	Method	Materials	Thickness	ϵ_{ref}	ϵ_{cal}	% Error
Ref [11]	Loaded waveguide technique and Clamped waveguide technique	Neoprene foam	-	1.40	1.41	1.6
		Carbon-filled rubber	-	10.57	10.84	2.5
		Carbon-filled polyethylene	-	3.22	3.28	1.9
		Conductive ABS-PVC	-	7.97	8.62	8.1
Ref [12]	EM simulations to measure the scattering (S) parameters	RT/Duroid	-	3.55	3.60	<2
		3D PLA (polylactide)	-	2.7	2.55	<5
Ref [13]	Reflection measurements of a loaded and unloaded CPW (coplanar waveguide) line sample holder	Teflon	1.6	1.95	2	2.5
		Polycarbonate	1.6	2.76	2.8	1.42
		RT/Duroid 6002	2.5	2.85	2.94	3.1
		FR-4 Epoxy	1.5	4.22	4.36	3.2
		RT/Duroid 6006	2.5	6.65	6.45	3.1
This work	Bayesian inversion method	Rogers RT/Duroid 5880	0.65	4.4	4.46	1.5
		FR4 Epoxy	1.5	2.2	2.17	1.0
		Rogers AD600	0.5	6.15	6.15	0.32

4. Conclusions

The Bayesian inversion method provides a measure of reliability in estimating the dielectric material properties because of the probabilistic approach. The presented Bayesian inversion method employs the measured scattering parameters to estimate the relative permittivity, material thickness, and MUT positioning error for several single-layer and three multi-layer materials. The measurements are carried out at Ka-band (26–40 GHz) using a standard gain horn antenna. The FR4 Epoxy, Rogers RT/Duriod 5880, and Rogers AD600 with relative permittivities 4.4, 2.2, and 6.15, and thicknesses of 1.52/0.78 mm, 0.65 mm, and 0.5 mm, respectively, are used in the measurement setup. The estimated model parameters showed 80% and above accuracy for all the presented cases. The confidence in the estimated model parameters has also been found in terms of eigenvectors. The proposed method and analysis can improve microwave imaging accuracy, non-destructive testing (NDT), and various quality control and security systems applications.

Author Contributions: Initial literature review and conceptualization, S.S. and G.G.G.; experimental setup and measurements, S.S.; MATLAB coding and procedure development, G.G.G., G.B. and H.N.; validation, and investigation, A.S.R., and G.B.; writing—original draft preparation, S.S. and H.N.; writing—review and editing, G.G.G., A.S.R., and G.B. All authors have read and agreed to the published version of the manuscript.

Funding: This research received no external funding.

Institutional Review Board Statement: Not applicable.

Informed Consent Statement: Not applicable.

Data Availability Statement: All data generated or analyzed during this study are included in this article.

Acknowledgments: The authors would like to thank the support of Santi Buitrago at Antenna Lab, Universitat Politècnica de Catalunya Barcelona Tech (UPC) Barcelona, for the equipment and measurements at Ka-band.

Conflicts of Interest: The authors declare no conflict of interest.

References

1. Zahm, O.; Cui, T.; Law, K.; Spantini, A.; Marzouk, Y. Certified dimension reduction in nonlinear Bayesian inverse problems. *Math. Comput.* **2022**, *91*, 1789–1835. [[CrossRef](#)]
2. Long, D.K.; Bangerth, W.; Handwerk, D.R.; Whitehead, C.B.; Shipman, P.D.; Finke, R.G. Estimating reaction parameters in mechanism-enabled population balance models of nanoparticle size distributions: A Bayesian inverse problem approach. *J. Comput. Chem.* **2022**, *43*, 43–56. [[CrossRef](#)] [[PubMed](#)]
3. Wang, K.; Bui-Thanh, T.; Ghattas, O. A randomized maximum a posteriori method for posterior sampling of high dimensional nonlinear Bayesian inverse problems. *SIAM J. Sci. Comput.* **2018**, *40*, A142–A171. [[CrossRef](#)]
4. Bardsley, J.M. *Computational Uncertainty Quantification for Inverse Problems*; SIAM: Philadelphia, PA, USA, 2018.
5. Tarantola, A. *Inverse Problem Theory and Methods for Model Parameter Estimation*; Society for Industrial and Applied Mathematics (SIAM): Philadelphia, PA, USA, 2005.
6. Dell'Aversana, P.; Bernasconi, G.; Miotti, F.; Rovetta, D. Joint inversion of rock properties from sonic, resistivity and density well-log measurements. *Geophys. Prospect.* **2011**, *59*, 1144–1154. [[CrossRef](#)]
7. Adler, J.; Lunz, S.; Verdier, O.; Schönlieb, C.B.; Öktem, O. Task adapted reconstruction for inverse problems. *Inverse Probl.* **2022**, *38*, 075006. [[CrossRef](#)]
8. Li, S.; Zhang, C.; Zhang, Z.; Zhao, H. A data-driven and model-based accelerated Hamiltonian Monte Carlo method for Bayesian elliptic inverse problems. *arXiv* **2021**, arXiv:2104.13070.
9. Huang, D.Z.; Huang, J.; Reich, S.; Stuart, A.M. Efficient Derivative-free Bayesian Inference for Large-Scale Inverse Problems. *arXiv* **2022**, arXiv:2204.04386. [[CrossRef](#)]
10. Xia, Y.; Zabarar, N. Bayesian multiscale deep generative model for the solution of high-dimensional inverse problems. *J. Comput. Phys.* **2022**, *455*, 111008. [[CrossRef](#)]
11. Munalli, D.; Qaseer, M.T.A.; Zoughi, R. Modified Waveguide-Based Method for Microwave Characterization of High-Loss Materials. *IEEE Trans. Instrum. Meas.* **2022**, *71*, 1–10. [[CrossRef](#)]
12. Alhassoon, K.; Malallah, Y.; Alcantar-Peña, J.J.; Kumar, N.; Daryoush, A.S. Broadband RF Characterization and Extraction of Material Properties in 3-D Printed Composite Substrates for Magnetically Tuned Circuits. *IEEE Trans. Microw. Theory Tech.* **2021**, *69*, 1703–1710. [[CrossRef](#)]

13. Nasr, A.M.H.; Nashashibi, A.Y.; Sarabandi, K. Ultrawideband Characterization of Complex Dielectric Constant of Planar Materials for 5G Applications. *IEEE Trans. Instrum. Meas.* **2021**, *70*, 1–11. [[CrossRef](#)]
14. Aretz-Nellesen, N.; Chen, P.; Grepl, M.A.; Veroy, K. A sequential sensor selection strategy for hyper-parameterized linear Bayesian inverse problems. In *Numerical Mathematics and Advanced Applications ENUMATH 2019*; Springer: Cham, Germany, 2021; pp. 489–497.
15. Hellmuth, K.; Klingenberg, C.; Li, Q.; Tang, M. Multiscale convergence of the inverse problem for chemotaxis in the Bayesian setting. *Computation* **2021**, *9*, 119. [[CrossRef](#)]
16. Myers, A.; Thiéry, A.H.; Wang, K.; Bui-Thanh, T. Sequential ensemble transform for Bayesian inverse problems. *J. Comput. Phys.* **2021**, *427*, 110055. [[CrossRef](#)]
17. González, M.; Almansa, A.; Tan, P. Solving inverse problems by joint posterior maximization with autoencoding prior. *SIAM J. Imaging Sci.* **2022**, *15*, 822–859. [[CrossRef](#)]
18. Aretz, N.; Chen, P.; Veroy, K. Sensor selection for hyper-parameterized linear Bayesian inverse problems. *PAMM* **2021**, *20*, e202000357. [[CrossRef](#)]
19. Monard, F.; Nickl, R.; Paternain, G.P. Statistical guarantees for Bayesian uncertainty quantification in nonlinear inverse problems with Gaussian process priors. *Ann. Stat.* **2021**, *49*, 3255–3298. [[CrossRef](#)]
20. Mohammad-Djafari, A. Regularization, Bayesian inference, and machine learning methods for inverse problems. *Entropy* **2021**, *23*, 1673. [[CrossRef](#)] [[PubMed](#)]

Disclaimer/Publisher’s Note: The statements, opinions and data contained in all publications are solely those of the individual author(s) and contributor(s) and not of MDPI and/or the editor(s). MDPI and/or the editor(s) disclaim responsibility for any injury to people or property resulting from any ideas, methods, instructions or products referred to in the content.